



**HAL**  
open science

## Programmed mechano-chemical coupling in reaction-diffusion active matter

Anis Senoussi, Jean-Christophe Galas, André Estévez-Torres

► **To cite this version:**

Anis Senoussi, Jean-Christophe Galas, André Estévez-Torres. Programmed mechano-chemical coupling in reaction-diffusion active matter. 2021. hal-03172911v1

**HAL Id: hal-03172911**

**<https://hal.sorbonne-universite.fr/hal-03172911v1>**

Preprint submitted on 18 Mar 2021 (v1), last revised 8 Nov 2022 (v2)

**HAL** is a multi-disciplinary open access archive for the deposit and dissemination of scientific research documents, whether they are published or not. The documents may come from teaching and research institutions in France or abroad, or from public or private research centers.

L'archive ouverte pluridisciplinaire **HAL**, est destinée au dépôt et à la diffusion de documents scientifiques de niveau recherche, publiés ou non, émanant des établissements d'enseignement et de recherche français ou étrangers, des laboratoires publics ou privés.

# Programmed mechano-chemical coupling in reaction-diffusion active matter

Anis Senoussi,<sup>\*</sup> Jean-Christophe Galas,<sup>\*</sup> and André Estevez-Torres<sup>\*</sup>

<sup>1</sup>

*Sorbonne Université, CNRS, Institut de Biologie Paris-Seine (IBPS), Laboratoire Jean Perrin  
(LJP), F-75005, Paris*

E-mail: [anis.senoussi@sorbonne-universite.fr](mailto:anis.senoussi@sorbonne-universite.fr); [jean-christophe.galas@sorbonne-universite.fr](mailto:jean-christophe.galas@sorbonne-universite.fr);  
[andre.estevez-torres@sorbonne-universite.fr](mailto:andre.estevez-torres@sorbonne-universite.fr)

## Abstract

Embryo morphogenesis involves a complex combination of pattern-forming mechanisms. However, classical *in vitro* patterning experiments explore only one mechanism at a time, thus missing coupling effects. Here, we conjugate two major pattern-forming mechanisms—reaction-diffusion and active matter—by integrating dissipative DNA/enzyme reaction networks within an active gel composed of cytoskeletal motors and filaments. We show that the strength of the flow generated by the active gel controls the mechano-chemical coupling between the two subsystems. We use this property to engineer the mechanical activation of chemical reaction networks both in time and space, thus mimicking key aspects of the polarization mechanism observed in *C. elegans* oocytes. We anticipate that reaction-diffusion active matter may be useful to investigate mechano-chemical transduction and to design new materials with life-like properties.

**Keywords:** DNA programming, active matter, morphogenesis, pattern formation, life-like material

**Short title:** Programmable reaction-diffusion active matter

18 Living embryos get their shape through a complex combination of chemical and phys-  
19 ical processes that take place out of equilibrium. Basically, biochemical reaction networks  
20 process information at particular points of space and time, while active gels generate me-  
21 chanical forces and flows.<sup>1</sup> These two generic processes are intertwined through diverse  
22 chemo-mechanical and mechano-chemical couplings and both continuously consume chem-  
23 ical energy. For instance, the pathway Rho GTPase brings about local contractions of the  
24 actomyosin cortex in *Xenopus*,<sup>2</sup> which regulates the cell cycle, while cytoplasmic flows of this  
25 same cortex trigger the PAR reaction network in *C. elegans*, inducing embryo polarization.<sup>3</sup>

26 The development of *in vitro* dissipative molecular systems is key to produce non-equilibrium  
27 materials and to investigate these processes in a controlled environment for testing theo-  
28 retical predictions.<sup>4,5</sup> On the chemical side, *in vitro* out-of-equilibrium reaction networks  
29 produce spatio-temporal concentration patterns through reaction or reaction-diffusion insta-  
30 bilities.<sup>6-14</sup> On the mechanical side, active gels made of cytoskeletal motors and filaments  
31 reconstituted *in vitro*<sup>4,15-24</sup> convert chemical energy into mechanical work and generate static  
32 patterns and flows through hydrodynamic instabilities.<sup>25</sup> More recently, efforts have focused  
33 on coupling reaction networks with active fluids and gels, resulting in redox-controlled self-  
34 oscillating gels<sup>26</sup> and DNA-controlled passive<sup>27</sup> and active gels.<sup>28-30</sup> However, so far, only  
35 one of the two systems could be maintained out of equilibrium, either the reaction network,<sup>26</sup>  
36 or the gel,<sup>27-31</sup> and thus only one of them could exhibit spatio-temporal self-organization.  
37 This constraint suppresses the rich variety of mechano-chemical couplings that are essential  
38 for pattern generation during development.<sup>1</sup> It thus constitutes a major limitation for the  
39 design of self-shaping materials inspired from embryogenesis.<sup>5</sup>

40 To create a functional mechano-chemical dissipative material we assembled two dissipa-  
41 tive molecular subsystems, a chemical and a mechanical one. The chemical subsystem is  
42 made of a network of DNA/enzyme reactions that produce single-stranded DNA (ssDNA)  
43 molecules<sup>13</sup> (Figure 1a). The mechanical subsystem is an active gel composed of bundles  
44 of protein filaments propelled by molecular motors<sup>15,17</sup> (Figure 1b). Each subsystem is

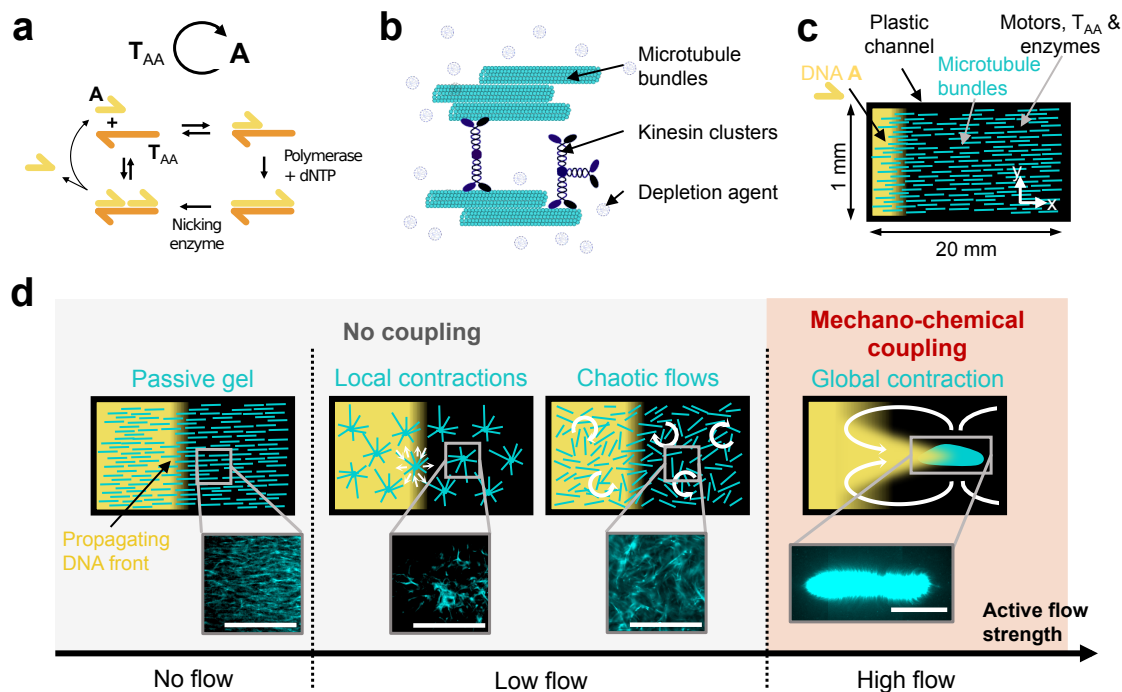


Figure 1: In a reaction-diffusion active matter system, the coupling between the mechanical and the chemical subsystem is controlled by the strength of the active flow. (a) Scheme of the chemical subsystem involving the autocatalytic amplification of DNA strand **A** in the presence of enzymes and template strand  $T_{AA}$ . Harpoon-ended arrows denote ssDNA. (b) Cartoon of the mechanical subsystem: an active gel formed by microtubules bundled together by a depletion agent and clusters of kinesin-1 motors. (c) Sketch of the channel in which the front propagation and the active gel dynamics were observed by fluorescence microscopy. Initially, **A** (yellow) is present only on the left side and the microtubule bundles (light blue) are aligned along  $x$ . (d) A mechano-chemical coupling between the two subsystems is achieved by increasing the strength of the flows generated by the active gel, which induces four different microtubule structures (light blue) and two DNA patterns (yellow). The white arrows represent the hydrodynamic flows generated by the active gel. Fluorescence images of the microtubules are represented for each morphology. Scale bars are 0.5 mm.

45 maintained out of equilibrium *via* the hydrolysis of high-energy compounds, respectively  
 46 deoxynucleosidetriphosphates (dNTPs) and adenosinetriphosphate (ATP).

47 The chosen chemical subsystem has four advantages. Firstly, due to DNA hybridization  
 48 rules, it can be easily reprogrammed into a variety of dissipative dynamics such as oscilla-  
 49 tions,<sup>32</sup> bistability and excitability.<sup>33</sup> Secondly, it can be maintained out of equilibrium in a  
 50 closed reactor for days.<sup>34</sup> Thirdly, working in water at pH 7, it is *a priori* compatible with  
 51 other biochemical reactions.<sup>35</sup> Lastly, it generates a variety of reaction-diffusion patterns

52 such as traveling fronts,<sup>36</sup> waves<sup>14</sup> and stationary patterns.<sup>37</sup> In a first series of experiments,  
53 the chemical subsystem encoded an autocatalytic loop that produces ssDNA species **A** —  
54 the node— in the presence of ssDNA **T<sub>AA</sub>** —the template—, a polymerase and a nicking  
55 enzyme<sup>13</sup> (Figure 1a).

56 In the mechanical subsystem, the bundles are constituted of stabilized microtubule fil-  
57 aments assembled together by attracting forces generated by the presence of a depletion  
58 agent<sup>17</sup> (Figure 1b). The motors are clusters of kinesin-1 and thus can bind several micro-  
59 tubules at once.<sup>†</sup> Such an active gel generates macroscopic flows that, depending on the  
60 concentration of motors and filaments, produce a diversity of microtubule morphologies:<sup>4,5</sup>  
61 local contractions,<sup>15</sup> corrugations,<sup>24</sup> chaotic flows,<sup>17</sup> and global contractions.<sup>21</sup> In the follow-  
62 ing, we demonstrate that, when mixed together, the two subsystems retain their ability to  
63 undergo, respectively, chemical and mechanical instabilities that generate spatio-temporal  
64 patterns. We further show that the strength of the active flow generated by the mechani-  
65 cal subsystem controls the mechanochemical coupling between the two subsystems. Finally,  
66 we take advantage of this property to design materials that mimic crucial aspects of a  
67 mechanochemical patterning mechanism observed in *C. elegans* embryo.

68 To check whether the two subsystems remained functional when combined in an opti-  
69 mized buffer (Figure S1), we tested the propagation of a DNA front through an active gel  
70 undergoing local contractions. To do so, a solution containing all the components of the  
71 chemical and mechanical subsystems, except the strand **A**, were filled into a microchannel.\*  
72 An initial condition containing the same solution supplemented with **A** was injected on the  
73 left side of the channel (Figure 1c). We recorded the spatiotemporal dynamics of each subsys-  
74 tem by fluorescence microscopy thanks to the presence of a DNA intercalator that becomes  
75 fluorescent upon binding to double-stranded DNA and of fluorescently-labeled microtubules  
76 (SI Methods). In the chemical subsystem, we observed the propagation of a front of DNA

---

<sup>†</sup>Two types of clusters were used: biotinylated kinesin-1 (from *D. melanogaster*) assembled together by streptavidin,<sup>15</sup> or clusters made from SNAPtag modified kinesin-1 (from *R. norvegicus*) that spontaneously multimerize<sup>24</sup> (SI Methods).

\*The experimental conditions for each figure are provided in Tables S2-S5.

77 fluorescence with constant velocity  $v_c = 20 \mu\text{m}/\text{min}$  across the whole length of the active gel,  
 78 *i.e.*  $> 1 \text{ cm}$  (Figures 1d, 2a, S2 and Movie S1). Concomitantly, in the mechanical subsystem  
 79 the microtubules contracted locally with a characteristic time  $\tau_m = 50 \text{ min}$  into aggregates  
 80 with a typical size of  $100 - 500 \mu\text{m}$ . The observation of a DNA front and microtubule ag-  
 81 gregates is in agreement with previous reports for each subsystem taken independently.<sup>15,36</sup>

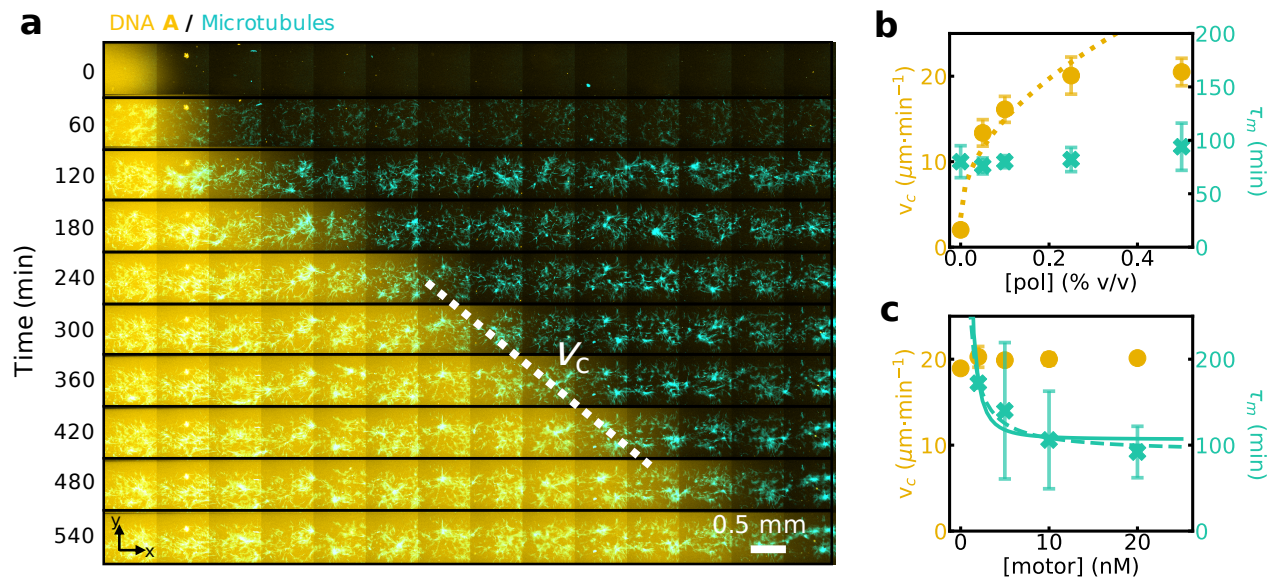


Figure 2: A DNA/enzyme reaction-diffusion front propagates normally inside a locally-contracting cytoskeletal active gel and the dynamics of each subsystem can be independently tuned. (a) Time-lapse 2-color image of the fluorescence intensities associated to species **A** (yellow) and to the microtubule network (light blue) (see also Movie S1). The dotted line indicates the velocity of the chemical front,  $v_c$ . Plots of  $v_c$  (yellow disks) and contraction time of the active gel,  $\tau_m$ , (blue crosses) for different concentrations of DNA polymerase (b) and motors (c). The lines are fits to the data with  $v_c \sim [\text{pol}]^{1/2}$  (dotted line),  $\tau_m \sim [\text{motor}]^{-1}$  (dashed line) and  $\tau_m \sim [\text{motor}]^{-2}$  (plain line). Error bars correspond to one standard deviation from a triplicate experiment.

82 When the active gel produces local contractions, the dynamics of each subsystem can  
 83 be independently tuned. Increasing the polymerase concentration, [pol], increases the front  
 84 velocity,  $v_c$ , until reaching a plateau at  $22 \mu\text{m}/\text{min}$  (Figure 2b). In these conditions, the  
 85 characteristic contraction time  $\tau_m$  remained constant. We find a scaling  $v_c \sim [\text{pol}]^{1/2}$ , in  
 86 agreement with previous results<sup>36</sup> and characteristic of Luther reaction-diffusion dynamics  
 87 where  $v_c \sim r_c^{1/2}$ , taking  $r_c \sim [\text{pol}]$  for the rate of the autocatalytic reaction as observed

88 in previous experiments.<sup>36</sup> In turn, when the motor concentration, [motor], increases,  $\tau_m$   
89 decreases until reaching a plateau at 100 min (Figure 2c) and the size of microtubule ag-  
90 gregates increases (Figure S3), while  $v_c$  remains constant. A hydrodynamic model of a  
91 contracting active gel<sup>5</sup> yields  $\tau_m^{-1} \sim \zeta([\text{motor}])$ , where  $\zeta$  is the strength of the gel activity,  
92 which depends on the motor concentration, and two scalings are found in the literature<sup>18,38</sup>  
93 yielding  $\tau_m \sim [\text{motor}]^{-\alpha}$ , with  $\alpha = 1, 2$  (Supplementary Text). Our data are compatible  
94 with both scalings (Figure 2c). In summary, Figure 2 shows that the two subsystems are  
95 both chemically and mechanically decoupled when the gel undergoes local contractions.

96 By varying the conditions, we can propagate the chemical front through active gels under-  
97 going other spatial instabilities associated with different active flow strengths, as sketched  
98 in Figure 1d. When the dGTP concentration was reduced (Figures S4-S5), chaotic flows  
99 were observed in the mechanical subsystem during several hours before local contractions  
100 occurred (Movie S2). Such flows did not modify the velocity of the chemical front because  
101 transport remained dominated by Brownian diffusion.\* When the length of microtubules  
102 was increased using taxol and the motor concentration reduced, the active gel formed corru-  
103 gations reminiscent of those previously reported in the absence of the chemical subsystem,<sup>24</sup>  
104 again without perturbing the chemical front (Movie S3).

105 In contrast, a dramatic perturbation of the front propagation was observed when the  
106 active gel underwent a global contraction, associated with large hydrodynamic flows (Fig-  
107 ures 3 and S6-S11 and Movie S4). Global contractions were observed for long microtubules  
108 and relatively high motor concentrations (Figure S7). When the gel contracted more rapidly  
109 than the front propagated, the front moved faster and we distinguished 4 phases (Figure 3c).  
110 During phase I, the active gel contracted rapidly towards the center of the channel, accelerat-  
111 ing until reaching a maximum velocity  $v_m = 400 \mu\text{m}/\text{min}$  at the end of phase I and dragging  
112 DNA along, which formed a detached DNA islet ahead of the front. During phase II the gel

---

\*The diffusivity of  $\mathbf{A}$  due to the active flow,  $D_f$ , was estimated to be 10-fold smaller than the Brownian diffusivity of  $\mathbf{A}$ ,  $D_A$ , and thus  $v_c \sim (D_A + D_f)^{1/2} \approx D_A^{1/2}$  corresponds to a purely reaction-diffusion front (Supplementary Text).



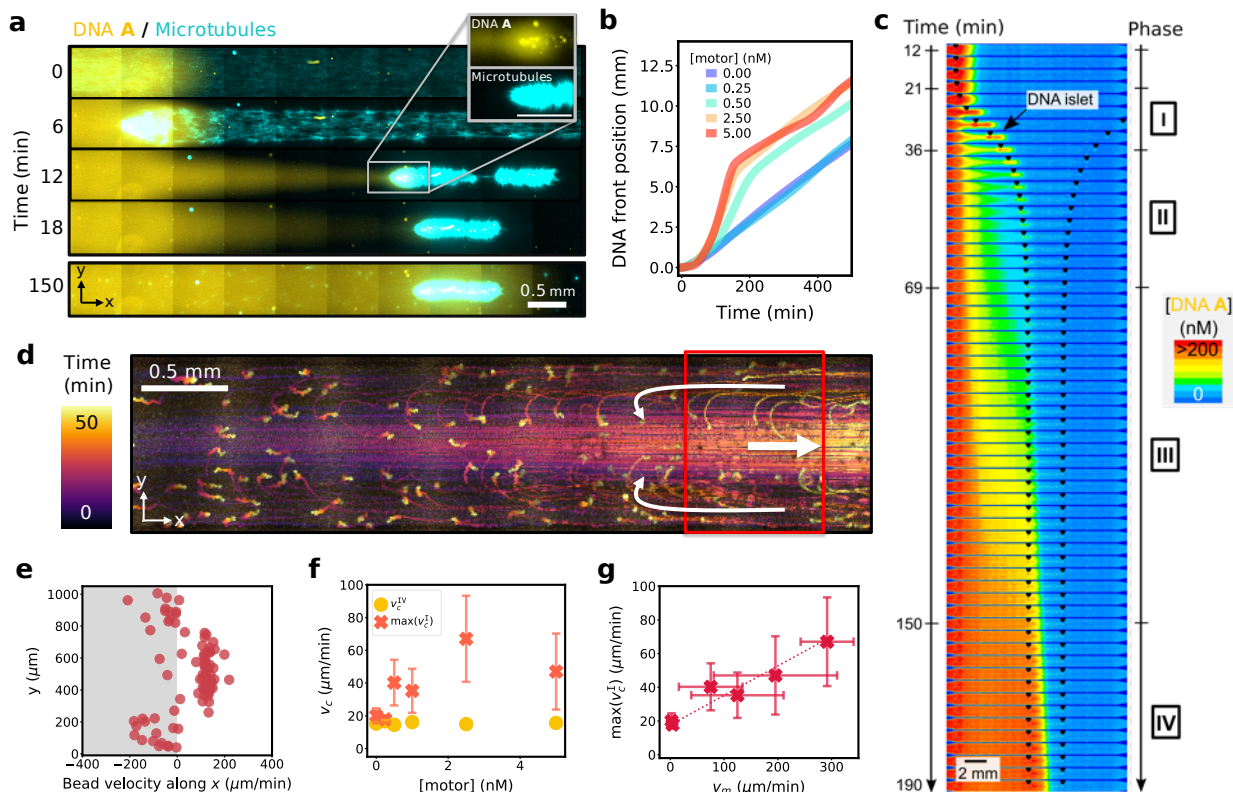


Figure 3: A globally-contracting active gel stretches and accelerates a reaction-diffusion front. (a) Time-lapse, 2-color fluorescence image with the DNA front in yellow and the microtubules in light blue. The inset shows the two fluorescence channels in separate images for the selected region. The white and yellow spots are dust particles concentrated by the contracting gel (see also Movie 4). (b) Position of the DNA front along  $x$  for different motor concentrations. (c) Time-lapse images of DNA fluorescence (color) at  $[\text{motor}] = 2.5$  nM and 3 min per image. The extremities of the contracting gel are indicated with black markers. Roman numerals indicate the 4 phases described in the text. (d) Stroboscopic image averaged over 50 min showing the trajectories of fluorescent beads during gel contraction, the white arrows indicate the sense of the flow (see also Movie 5) and (e) plot of the bead velocity along  $x$  across the width of the channel for the beads in the red rectangle, 25 min after the beginning of the contraction. (f) Maximal front velocity during phase I (crosses) and steady-state velocity during phase IV (disks) for different motor concentrations. (g) Maximal front velocity during phase I *vs.* maximal gel contraction velocity. Error bars correspond to one standard deviation from a triplicate experiment.

113 decelerated and the DNA islet was diluted in the  $xy$  plane resulting in a front with a skewed  
 114 profile 5-fold wider than the initial one (Figure S6). Throughout phases I and II the Péclet  
 115 number was greater than 1 (Figure S8), indicating that active convection predominated over  
 116 diffusion. Finally, when the active gel stopped contracting, the DNA front slowly recovered

117 a sigmoidal shape (phase III, Figure S6) and eventually reached a steady state with constant  
118 velocity and width (phase IV).

119 In a control experiment with a passive dye, only phases I and II were observed, indicat-  
120 ing that reaction was necessary for phases III and IV and that DNA islet formation was not  
121 related to the binding of DNA to the active gel (Figure S10). We confirmed the last interpre-  
122 tation by adding passive brownian beads to measure the hydrodynamic flow induced during  
123 contraction. We observed two counter-rotating fluid rolls, symmetric along the central axis  
124 of the channel,  $x$ , and producing water flows along  $x$  that reached  $+150 \mu\text{m}/\text{min}$  in the  
125 center of the channel and  $-100 \mu\text{m}/\text{min}$  at its borders (Figures 3d,e and S11 and Movie S5).  
126 Taken together, these results indicate that the stretching of the concentration profile of **A**  
127 leading to the formation of the DNA islet during phase I was a purely hydrodynamic process.

128 The active gel contraction velocity,  $v_m$ , was a sigmoidal function of the motor concentra-  
129 tion (Figure S7). We quantified the two main regimes of front propagation with  $\max(v_c^I)$  the  
130 maximal velocity during phase I and  $v_c^{IV}$  the velocity at steady state in phase IV. Figure 3f  
131 shows that the former strongly depended on the motor concentration while the latter was  
132 independent. Finally, the linear relationship between  $\max(v_c^I)$  and  $v_m$  is consistent with the  
133 observation of a convection-dominated transport during phase I (Figure 3g). Taken together,  
134 these results show that when the flows generated by the active gel are sufficiently fast there  
135 is a mechano-chemical coupling between the gel and the reaction-diffusion front. This cou-  
136 pling happens through hydrodynamics and can be interpreted as a time-dependent Taylor  
137 dispersion.<sup>39</sup>

138 We have just seen that active flows can significantly modify heterogeneous concentration  
139 profiles present in the chemical subsystem. Can they induce an asymmetry in an initially  
140 homogeneous chemical subsystem? This is what happens in the *C. elegans* embryo, where  
141 the active flow generated by the actomyosin cortex breaks the symmetry of an initially  
142 homogeneous distribution of PAR-proteins. Later, this asymmetry is amplified by a PAR-  
143 dependent bistable reaction network, leading to embryo polarization.<sup>3</sup> The reaction-diffusion

144 active matter system developed here is a good candidate to mimic this process in a synthetic  
145 material. To do so, we first need to implement a mechanism that couples a variation in  
146 the microtubule concentration with a change in the concentration of a DNA species that is  
147 initially homogeneously distributed and second to engineer a chemical network that amplifies  
148 this concentration change.

149 The first requirement was fulfilled by attaching DNA strands to  $\sim 30 \mu\text{m}$  diameter hydro-  
150 gel beads, which were trapped by the microtubule mesh and concentrated during contraction.  
151 The second condition was satisfied by engineering a chemical subsystem whose kinetics de-  
152 pend on the concentration of DNA-bead conjugates, and thus on the contraction state of the  
153 gel. More precisely, the DNA autocatalytic loop was split into two nodes, **B** and **D**, that  
154 cross-activate each other thanks to the templates  $\mathbf{T}_{BD}$  and  $\mathbf{T}_{DB}$  (Figure 4a). By attaching  
155 each of these templates to a set of hydrogel beads and supplementing the medium with an  
156 exonuclease that degrades **B** and **D** (Figure 4a) the cross-catalysis kinetics become diffusion-  
157 controlled<sup>40</sup> and thus should depend on bead density. As a result, the beads brought together  
158 in a contracted gel should activate faster, producing DNA that light them up in the presence  
159 of a DNA intercalator dye (Figure 4b). Indeed, when both types of beads were embedded  
160 in the active gel in the presence of a homogeneous, low concentration of **D**, they first reached  
161 a high density as the gel contracted and later they became fluorescent (Figures 4c,d, S13 and  
162 Movie S6). In the absence of contraction, the bead fluorescence amplification was delayed  
163 (Figure S12) and its final amplitude reduced, both by a factor 2 (Figure 4d). As expected  
164 for diffusion-controlled kinetics, the mechano-chemical DNA amplification dynamics slowed  
165 down with increasing exonuclease concentration (Figure 4d).

166 To show that the activated beads may trigger downstream reactions in solution, the  
167 previous system was supplemented with freely-diffusing templates  $\mathbf{T}_{BA}$  and  $\mathbf{T}_{AA}$ , that re-  
168 spectively convert **B** into **A** and sustain the autocatalytic reaction of **A** described earlier.  
169 In addition, to suppress the undesired self-activation of  $\mathbf{T}_{AA}$  a repressor strand  $\mathbf{R}_A$  was  
170 added<sup>33</sup> (Figure S15). In the presence of motors, the beads were all activated within 1 h at

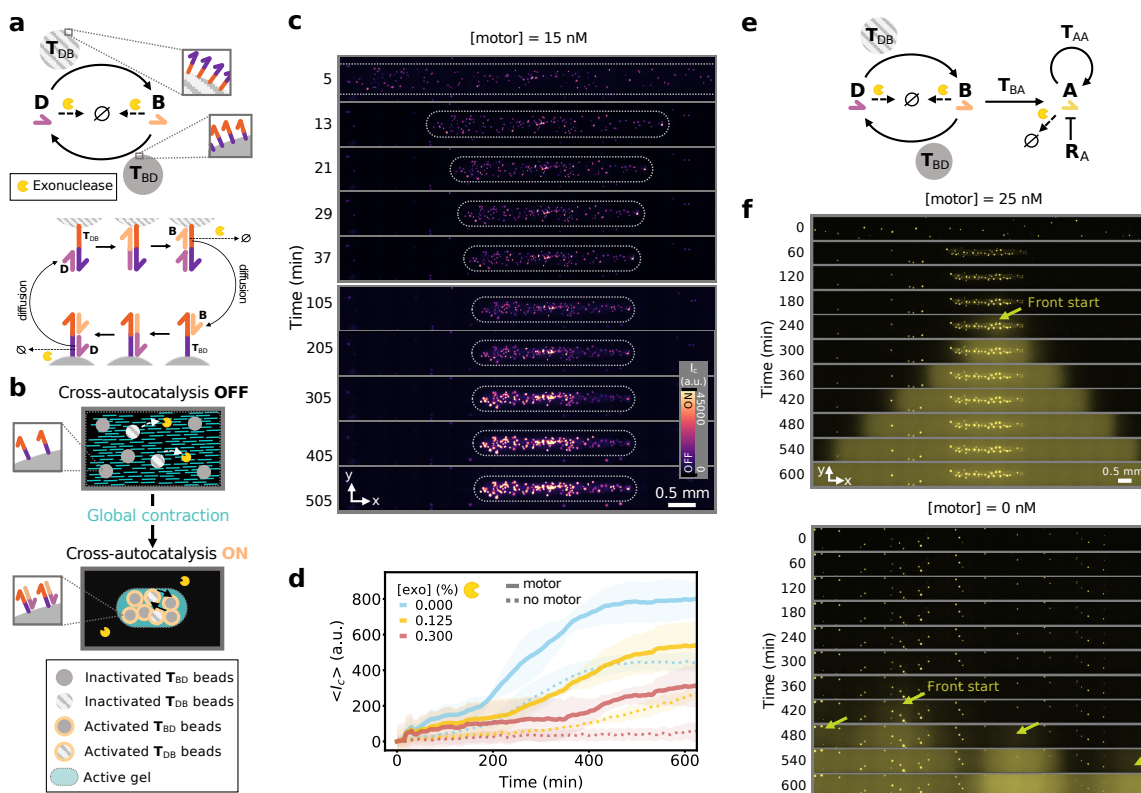


Figure 4: A globally-contracting active gel triggers the activation of downstream reaction networks with temporal and spatial control. (a) Scheme of the cross-autocatalytic DNA/enzyme network (top). Plain and dotted arrows indicate activation and degradation reactions, respectively. Harpoon-ended arrows correspond to ssDNA and disks indicate hydrogel beads carrying templates  $T_{ij}$ . Detailed mechanism of bead activation where the diffusion of **B** and **D** between beads is indicated (bottom). (b) Sketch of the mechano-chemical activation of the reaction network in panel a through the contraction of the active gel (light blue) that brings the hydrogel beads (disks) close together, speeding up cross-catalysis. (c) Time-lapse images of DNA fluorescence from the template-bearing beads embedded in the active gel in the presence of motors. White dotted lines indicate the borders of the active gel and the channel walls are depicted in gray. (d) Average DNA fluorescence over the whole channel *vs.* time in the absence (dotted line) and in the presence (plain line) of motors for different exonuclease concentrations (colors). (e) Scheme of the bead-associated cross-autocatalytic network coupled to the autocatalysis of **A** in solution. Disks indicate templates linked to hydrogel beads. The blunt-ended arrow indicates repression. (f) Time-lapse images of DNA fluorescence in the channel for the network in panel e, in the presence (top) and in the absence (bottom) of motors. The bright spots are the beads, the arrows indicate the start of the fronts of **A**, in yellow.

171 the center of the channel, where the gel contracted, and they triggered a controlled front of  
172 **A** that propagated from the center of the channel to its extremities (Figures 4f and S14-S15  
173 and Movie S7). In contrast, in the absence of gel contraction, the beads randomly activated  
174 over the course of 5h, which was followed by the uncontrolled amplification of **A**. Taken  
175 together, these results demonstrate that mechano-chemical coupling can be engineered to  
176 trigger either temporal or spatio-temporal chemical instabilities in a synthetic material.

177 The coupling of chemical and mechanical self-organization is a key ingredient of biological  
178 complexity, in particular during embryogenesis. We have demonstrated that it is possible to  
179 couple two archetypal examples of these mechanisms, reaction-diffusion and active matter, in  
180 a synthetic material. Our design is modular because it relies on two distinct subsystems with  
181 well-characterized and predictable spatiotemporal behaviors: DNA/enzyme reactions and ki-  
182 nesin/microtubule active gels. Considered independently, each subsystem reveals complex  
183 dynamics and macroscopic organizations which are subject to intense scrutiny.<sup>14,15,17,19,21,24,35,37</sup>  
184 When mixed-together, the coupling strength between the two subsystems is set by the mag-  
185 nitude of the flow generated by the active gel. As a result, this system may be useful for  
186 investigating self-organization when chemical and mechanical out-of-equilibrium processes  
187 are intertwined. Finally, reaction-diffusion active matter provides a framework for the ratio-  
188 nal engineering of functional out-of-equilibrium materials with life-like properties. On the  
189 one hand, it could be advantageously combined with the wide array of methods in DNA nan-  
190 otechnology, such as nanostructure design,<sup>41</sup> logic gates,<sup>11</sup> analyte detection<sup>42</sup> or hydrogel  
191 swelling.<sup>27</sup> On the other hand, by using DNA-motor conjugates<sup>28-30</sup> or photosensitive mo-  
192 tors<sup>43</sup> the system is extendable to chemo-mechanical as well as photo-mechanical couplings.

## 193 Acknowledgements

194 We thank H. Berthoumieux, V. Bormuth, M. Elez, A. Genot, G. Gines, N. Lobato-Dauzier,  
195 A. Maitra, L. Robert, Y. Rondelez and R. Voituriez for insightful discussions and K. Furuta

196 and Z. Gueroui for their kind gift of kinesin plasmids. This work has been funded by the  
197 European Research Council (ERC) under the European's Union Horizon 2020 programme  
198 (grant No 770940, A.E.-T.), by the Ville de Paris Emergences programme (Morphoart, A.E.-  
199 T.) and by MITI CNRS (J.-C. G.). The data that support the findings of this study are  
200 available from the corresponding author upon reasonable request.

## 201 **References**

- 202 (1) Gross, P.; Kumar, K. V.; Grill, S. W. How Active Mechanics and Regulatory Biochem-  
203 istry Combine to Form Patterns in Development. *Annual Review of Biophysics* **2017**,  
204 *46*, 337–356.
- 205 (2) Bement, W. M.; Leda, M.; Moe, A.; Kita, A.; Larson, M.; Golding, A.; Pfeuti, C.;  
206 Su, K.-C.; Miller, A.; Goryachev, A.; von Dassow, G. Activator–inhibitor coupling  
207 between Rho signalling and actin assembly makes the cell cortex an excitable medium.  
208 *Nature Cell Biology* **2015**, *17*, 1471–1483.
- 209 (3) Goehring, N. W.; Trong, P. K.; Bois, J. S.; Chowdhury, D.; Nicola, E. M.; Hyman, A. A.;  
210 Grill, S. W. Polarization of PAR proteins by advective triggering of a pattern-forming  
211 system. *Science* **2011**, *334*, 1137–1141.
- 212 (4) Needleman, D.; Dogic, Z. Active matter at the interface between materials science and  
213 cell biology. *Nature reviews materials* **2017**, *2*, 17048.
- 214 (5) Senoussi, A.; Vyborna, Y.; Berthoumieux, H.; Galas, J.-C.; Estevez-Torres, A. In *Out-*  
215 *of-Equilibrium Supramolecular Systems and Materials*; Giuseppone, N., Walther, A.,  
216 Eds.; Wiley-VCH, in press.
- 217 (6) Epstein, I.; Pojman, J. A. *An introduction to nonlinear chemical reactions*; Oxford  
218 University Press: New York, 1998.

- 219 (7) Isalan, M.; Lemerle, C.; Serrano, L. Engineering gene networks to emulate *Drosophila*  
220 embryonic pattern formation. *PLoS biology* **2005**, *3*.
- 221 (8) Karzbrun, E.; Tayar, A. M.; Noireaux, V.; Bar-Ziv, R. H. Programmable on-chip DNA  
222 compartments as artificial cells. *Science* **2014**, *345*, 829–832.
- 223 (9) Nakajima, M.; Imai, K.; Ito, H.; Nishiwaki, T.; Murayama, Y.; Iwasaki, H.; Oyama, T.;  
224 Kondo, T. Reconstitution of Circadian Oscillation of Cyanobacterial KaiC Phosphory-  
225 lation in Vitro. *Science* **2005**, *308*, 414–415.
- 226 (10) Loose, M.; Fischer-Friedrich, E.; Ries, J.; Kruse, K.; Schwille, P. Spatial regulators  
227 for bacterial cell division self-organize into surface waves in vitro. *Science* **2008**, *320*,  
228 789–792.
- 229 (11) Zhang, D. Y.; Seelig, G. Dynamic DNA nanotechnology using strand-displacement  
230 reactions. *Nature chemistry* **2011**, *3*, 103.
- 231 (12) Chirieleison, S. M.; Allen, P. B.; Simpson, Z. B.; Ellington, A. D.; Chen, X. Pattern  
232 transformation with DNA circuits. *Nature chemistry* **2013**, *5*, 1000.
- 233 (13) Montagne, K.; Plasson, R.; Sakai, Y.; Fujii, T.; Rondelez, Y. Programming an in vitro  
234 DNA oscillator using a molecular networking strategy. *Molecular systems biology* **2011**,  
235 *7*.
- 236 (14) Padirac, A.; Fujii, T.; Estévez-Torres, A.; Rondelez, Y. Spatial waves in synthetic  
237 biochemical networks. *Journal of the American Chemical Society* **2013**, *135*, 14586–  
238 14592.
- 239 (15) Nedelec, F.; Surrey, T.; Maggs, A. C.; Leibler, S. Self-organization of microtubules and  
240 motors. *Nature* **1997**, *389*, 305.
- 241 (16) Bendix, P. M.; Koenderink, G. H.; Cuvelier, D.; Dogic, Z.; Koeleman, B. N.;  
242 Briehar, W. M.; Field, C. M.; Mahadevan, L.; Weitz, D. A. A quantitative analysis

- 243 of contractility in active cytoskeletal protein networks. *Biophysical journal* **2008**, *94*,  
244 3126–3136.
- 245 (17) Sanchez, T.; Chen, D. T.; DeCamp, S. J.; Heymann, M.; Dogic, Z. Spontaneous motion  
246 in hierarchically assembled active matter. *Nature* **2012**, *491*, 431.
- 247 (18) Foster, P. J.; Fürthauer, S.; Shelley, M. J.; Needleman, D. J. Active contraction of  
248 microtubule networks. *Elife* **2015**, *4*, e10837.
- 249 (19) Wu, K.-T.; Hishamunda, J. B.; Chen, D. T.; DeCamp, S. J.; Chang, Y.-W.; Fernández-  
250 Nieves, A.; Fraden, S.; Dogic, Z. Transition from turbulent to coherent flows in confined  
251 three-dimensional active fluids. *Science* **2017**, *355*, eaal1979.
- 252 (20) Kumar, N.; Zhang, R.; de Pablo, J. J.; Gardel, M. L. Tunable structure and dynamics  
253 of active liquid crystals. *Science advances* **2018**, *4*, eaat7779.
- 254 (21) Torisawa, T.; Taniguchi, D.; Ishihara, S.; Oiwa, K. Spontaneous formation of a glob-  
255 ally connected contractile network in a microtubule-motor system. *Biophysical journal*  
256 **2016**, *111*, 373–385.
- 257 (22) Ideses, Y.; Erukhimovitch, V.; Brand, R.; Jourdain, D.; Hernandez, J. S.; Gabinet, U.;  
258 Safran, S.; Kruse, K.; Bernheim-Groswasser, A. Spontaneous buckling of contractile  
259 poroelastic actomyosin sheets. *Nature communications* **2018**, *9*, 2461.
- 260 (23) Roostalu, J.; Rickman, J.; Thomas, C.; Nédélec, F.; Surrey, T. Determinants of polar  
261 versus nematic organization in networks of dynamic microtubules and mitotic motors.  
262 *Cell* **2018**, *175*, 796–808.
- 263 (24) Senoussi, A.; Kashida, S.; Voituriez, R.; Galas, J.-C.; Maitra, A.; Estevez-Torres, A.  
264 Tunable corrugated patterns in an active nematic sheet. *Proceedings of the National*  
265 *Academy of Sciences* **2019**, *116*, 22464–22470.



- 266 (25) Marchetti, M. C.; Joanny, J.-F.; Ramaswamy, S.; Liverpool, T. B.; Prost, J.; Rao, M.;  
267 Simha, R. A. Hydrodynamics of soft active matter. *Reviews of Modern Physics* **2013**,  
268 *85*, 1143.
- 269 (26) Yoshida, R.; Takahashi, T.; Yamaguchi, T.; Ichijo, H. Self-oscillating gel. *Journal of*  
270 *the American Chemical Society* **1996**, *118*, 5134–5135.
- 271 (27) Cangialosi, A.; Yoon, C.; Liu, J.; Huang, Q.; Guo, J.; Nguyen, T. D.; Gracias, D. H.;  
272 Schulman, R. DNA sequence–directed shape change of photopatterned hydrogels via  
273 high-degree swelling. *Science* **2017**, *357*, 1126–1130.
- 274 (28) Wollman, A. J.; Sanchez-Cano, C.; Carstairs, H. M.; Cross, R. A.; Turberfield, A. J.  
275 Transport and self-organization across different length scales powered by motor proteins  
276 and programmed by DNA. *Nature nanotechnology* **2014**, *9*, 44.
- 277 (29) Sato, Y.; Hiratsuka, Y.; Kawamata, I.; Murata, S.; Nomura, S.-i. M. Micrometer-sized  
278 molecular robot changes its shape in response to signal molecules. *Sci. Robot* **2017**, *2*.
- 279 (30) Keya, J. J.; Suzuki, R.; Kabir, A. M. R.; Inoue, D.; Asanuma, H.; Sada, K.; Hess, H.;  
280 Kuzuya, A.; Kakugo, A. DNA-assisted swarm control in a biomolecular motor system.  
281 *Nature communications* **2018**, *9*, 453.
- 282 (31) Bertrand, O. J. N.; Fygenson, D. K.; Saleh, O. A. Active, motor-driven me-  
283 chanics in a DNA gel. *Proceedings of the National Academy of Sciences* **2012**,  
284 *10.1073/pnas.1208732109*.
- 285 (32) Fujii, T.; Rondelez, Y. Predator–prey molecular ecosystems. *ACS nano* **2012**, *7*, 27–34.
- 286 (33) Montagne, K.; Gines, G.; Fujii, T.; Rondelez, Y. Boosting functionality of synthetic  
287 DNA circuits with tailored deactivation. *Nature communications* **2016**, *7*, 13474.

- 288 (34) Urtel, G.; Van Der Hofstadt, M.; Galas, J.-C.; Estevez-Torres, A. rEXPAR: an isother-  
289 mal amplification scheme that is robust to autocatalytic parasites. *Biochemistry* **2019**,  
290 *58*, 2675–2681.
- 291 (35) Van Der Hofstadt, M.; Galas, J.-C.; Estevez-Torres, A. Spatiotemporal Patterning of  
292 Living Cells with Extracellular DNA Programs. *ACS nano* **2020**,
- 293 (36) Zadorin, A. S.; Rondelez, Y.; Galas, J.-C.; Estevez-Torres, A. Synthesis of pro-  
294 grammable reaction-diffusion fronts using DNA catalyzers. *Physical review letters* **2015**,  
295 *114*, 068301.
- 296 (37) Zadorin, A. S.; Rondelez, Y.; Gines, G.; Dilhas, V.; Urtel, G.; Zambrano, A.; Galas, J.-  
297 C.; Estevez-Torres, A. Synthesis and materialization of a reaction-diffusion French flag  
298 pattern. *Nature chemistry* **2017**, *9*, 990.
- 299 (38) Martínez-Prat, B.; Ignés-Mullol, J.; Casademunt, J.; Sagués, F. Selection mechanism  
300 at the onset of active turbulence. *Nature physics* **2019**, *15*, 362.
- 301 (39) Vedel, S.; Bruus, H. Transient Taylor–Aris dispersion for time-dependent flows in  
302 straight channels. *Journal of Fluid Mechanics* **2011**, *691*, 95–122.
- 303 (40) Gines, G.; Zadorin, A.; Galas, J.-C.; Fujii, T.; Estevez-Torres, A.; Rondelez, Y. Micro-  
304 scopic agents programmed by DNA circuits. *Nature nanotechnology* **2017**, *12*, 351.
- 305 (41) Jones, M. R.; Seeman, N. C.; Mirkin, C. A. Programmable materials and the nature of  
306 the DNA bond. *Science* **2015**, *347*, 1260901.
- 307 (42) Zhao, Y.; Chen, F.; Li, Q.; Wang, L.; Fan, C. Isothermal Amplification of Nucleic  
308 Acids. *Chemical Reviews* **2015**, *115*, 12491–12545.
- 309 (43) Ross, T. D.; Lee, H. J.; Qu, Z.; Banks, R. A.; Phillips, R.; Thomson, M. Controlling  
310 organization and forces in active matter through optically defined boundaries. *Nature*  
311 **2019**, *572*, 224–229.